J Nanopart Res (2020) 22: 1
https://doi.org/10.1007/s11051-019-4718-8

RESEARCH PAPER

Patterned arrays of assembled nanoparticles prepared by interfacial assembly and femtosecond laser fabrication

Chengpeng Jiang · Daiki Oshima · Satoshi Iwata · Philip W. T. Pong · Takeshi Kato

Received: 28 March 2019 / Accepted: 20 November 2019 / Published online: 21 December 2019

Abstract Creating shape-defined structures of inorganic nanoparticles in a maskless and template-free fashion would advance the engineering of nanoparticle-based devices and structures with desired configurations for various applications. In this work, a novel fabrication protocol combining bottom-up interfacial assembly and subtractive laser patterning was developed for creating patterned arrays of assembled nanoparticles. A solid film of magnetic nanoparticles (10 nm, monodisperse $CoFe_2O_4$) was assembled as a nanoparticle film (thickness less than 100 nm) on liquid interface under guiding field, and it was further transferred to Si substrate followed by selective material removal using femtosecond laser pulses, producing patterned arrays (typical size of 3 μm) of assembled nanoparticles. The size, shape, and arrangement of the patterned arrays were finely regulated by adjusting the laser pulse energy and laser scanning path. The magnetization behavior and magnetic anisotropy of the patterned arrays differ from those of the nanoparticle-assembled film, as reflected by the changes of coercivity and squareness along the out-of-plane direction. The presented fabrication protocol is compatible with microelectronic fabrication techniques and can be applied to various inorganic nanoparticles.

Keywords Interfacial assembly · Femtosecond laser fabrication · Nanoparticle patterning · Magnetic properties · Collective properties

C. Jiang · D. Oshima · S. Iwata
Institute of Materials and Systems for Sustainability, Nagoya University, Nagoya 464-8603, Japan

P. W. T. Pong (✉)
Department of Electrical and Electronic Engineering, The University of Hong Kong, Hong Kong, China
e-mail: ppong@eee.hku.hk

T. Kato (✉)
Department of Electronics, Nagoya University, Nagoya 464-8603, Japan
e-mail: takeshik@nuee.nagoya-u.ac.jp

Present Address:
C. Jiang
Zhejiang Lab, Hangzhou 310000, China

Introduction

Patterning inorganic nanoparticles from their assemblies is of scientific interest and practical significance for developing novel fabrication strategies to build nanoparticle-based structures and devices in a bottom-up manner (Zhang et al. 2017; Boles et al. 2016). Functional nanoparticles, including metal oxides, metal sulfides, and quantum dots, have been extensively explored to be fabricated into different structures towards their material-specific applications in magnetics, optics, plasmonics, and nanorobotics (Wang 2008; Lin et al. 2018; Polavarapu and Liz-Marzán 2013; Cheang and Kim 2015). Patterned structures of nanoparticles with well-defined geometry are intriguing materials since the interparticle interactions and the collective properties can be finely tuned by controlling the size, shape,

arrangement, and composition of the constituent nanoparticles (Lin et al. 2018; Toulemon et al. 2016b).

In literature, various strategies ranging from template-guided assembly, entropy-dictated ordering, drop-on-demand deposition, to molecular organization have been developed to create patterns and arrays of assembled nanoparticles as desired. Photo- and electron-beam lithography methods were applied to construct auxiliary templates for confining the capillary assembly of colloidal nanoparticles, achieving defined placement of nanoparticles at micron or sub-micron scale, though the fabrication process needs predesigned masks or expensive facilities (Wen et al. 2015, 2017; Flauraud et al. 2017). Soft lithography routes exemplified by micro-contact printing and nano-imprinting techniques allow parallel patterning of assembled nanoparticles over large areas, but these techniques require nanoparticle functionalization and master stamp preparation (Gassensmith et al. 2013; Jie et al. 2012; Paik et al. 2017). Inkjet and aerosol jet printing approaches enable the maskless preparation of nanoparticle microstructures on planar and non-planar surfaces by regulating the printing and dewetting process of nanoparticle ink, with the nanoparticle chemistry and ink properties being tailored accordingly (You et al. 2015; Mahajan et al. 2013). Recently, biological and molecular materials such as DNA origami, engineered cell/virus, biofilms, and supramolecules have been used as scaffolds or linkers to program the nanoparticle clusters and arrays, allowing complex superlattices and hierarchical structures with prescribed spatiotemporal configurations to be assembled, but this state-of-the-art method is limited in feasibility, versatility, and scalability (Wang et al. 2018; Tian et al. 2015; O'Brien et al. 2016). As a maskless fabrication approach, femtosecond laser irradiation has advantages of ultra-short pulse width, reduced heat diffusion, and high peak intensity, and it is used for generating inorganic nanoparticles, fabricating sub-wavelength periodic structures, inducing fusion reactions, modifying material properties, and improving device performance (Stratakis et al. 2009; Okamoto et al. 2019; Kudryashov et al. 2018; Ionin et al. 2014; Lan et al. 2019). By a proper combination of femtosecond laser fabrication with nanoparticle self-assembly (Chiang et al. 2019; Catone et al. 2018), reduction or sintering of nanoparticles was induced and coalesced microstructures were formed in additive fashion (Son et al. 2011; Lee et al. 2014; Kang et al. 2011). In this case, the nanoparticles used for laser irradiation are limited to noble metals and low oxidation-potential metal oxides. However, utilizing femtosecond laser for subtractive ablation of assembled nanoparticles without changing the morphology or properties of nanoparticles has been scarcely reported.

Herein, a versatile fabrication protocol combining low-cost interfacial assembly and femtosecond laser patterning was developed to produce patterned arrays of assembled nanoparticles from nanoparticle-assembled film (Fig. 1). Magnetic nanoparticles capped by organic surfactant were used as the building blocks. Different types of patterned arrays were prepared and characterized. Micro patterns of QR code were also created as information carrier. Collective magnetic properties of the patterned square arrays were measured to study the magnetic anisotropy originating from nanoparticle organization. The presented fabrication protocol is maskless and template-free without involving lithography or vacuum fabrication, and it can be extended to various inorganic nanoparticles for fundamental research and device applications (Wen et al. 2017; Dong et al. 2010; Jiang et al. 2017a, b).

Experimental

Nanoparticle synthesis

$CoFe_2O_4$ nanoparticles were synthesized based on our previous protocol with slight modifications (Jiang et al. 2017a). Organometallic precursors, reducing agent, and surfactant were mixed with organic solvent and the mixture were heated stepwise (120 °C for 10 min, 200 °C for 1.5 h, 300 °C for 1 h) at a ramp of 5 °C min^{-1} under N_2 flow along with magnetic stirring. After cooling to room temperature, fourfold acetone served as antisolvent was added into the black colloidal solution, and the precipitated materials were dispersed in chloroform. This purification operation was repeated three times. The final product was dissolved in a mixture of toluene and hexane (volume ratio 1:1).

Nanoparticle assembly

One drop (15 μl) of diluted nanoparticle solution (25 mg mL^{-1}) was deposited onto the surface of Milli-Q water contained in a glass trough (4-cm petri-dish), producing a liquid film on water subphase. A glass lid was covered on the glass trough and a magnetic field

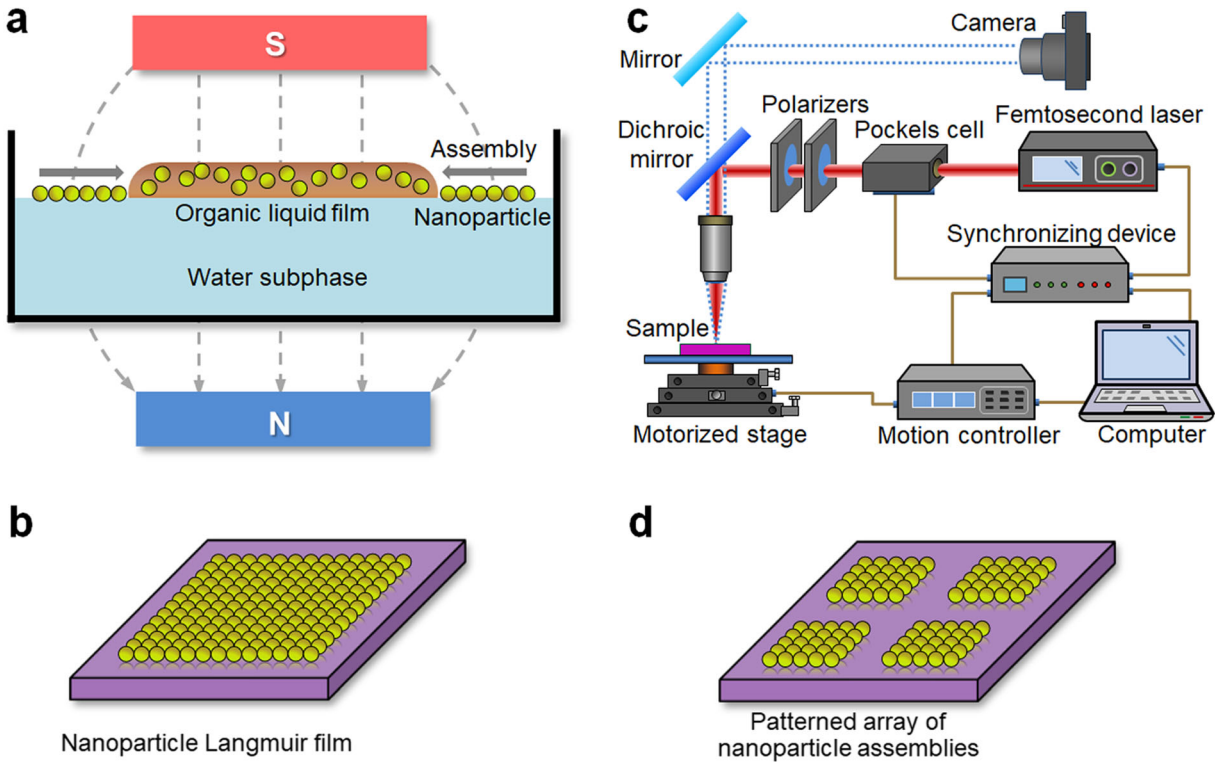

Fig. 1 Experimental setup for interfacial assembly of magnetic nanoparticles under guiding field (**a**); nanoparticle-assembled film prepared by interfacial assembly (**b**); experimental setup for subtractive patterning of assembled nanoparticles using femtosecond laser pulses (**c**); patterned array of assembled nanoparticles fabricated by femtosecond laser pulses (**d**)

(160 Oe) was applied perpendicular to the water surface. Upon evaporation of the organic solvent (~ 3 min), a solid film floating on water surface was obtained and it was then transferred to Si substrate (5 mm × 5 mm). This film attached on Si surface was further heated at 60 °C for 10 min to remove residual solvent.

Laser patterning

The Si substrate coated with nanoparticle-assembled film was mounted on a 3-axis motorized translation stage. To create patterns of assembled nanoparticles, a femtosecond laser system (IMRA μjewel D-1000, laser wavelength 1041 nm, pulse duration 550 fs) equipped with ventilation tubes was employed. Synchronization between the translation stage and the switched laser pulses was coordinated by a position synchronized output (PSO) device. The laser beam was focused by a × 20 objective lens. The spatial profile of the focused laser spot, which was analyzed with a CCD camera, is nearly Gaussian. The calculated diameter of the focused laser spot based on the diffraction limit of the microscopy system is 3.1 μm (Boyd 2003). The laser pulse energy was tuned for each run to achieve ablating nanoparticles but not to damage the Si surface. For continuously creating patterned arrays, the laser pulse frequency and the laser scanning speed were set to 10 kHz and 10 mm s^{-1}, respectively. For discretely creating antidots and QR codes, these two parameters were slowed down to 1 kHz and 1 mm s^{-1}, respectively. Post-fabrication processing was performed by ultrasonicating the sample in toluene for 5 min.

Characterization

Transmission electron microscopy (TEM) was performed using a Philips CM-100 TEM. The sample for TEM imaging was prepared by dropcasting the nanoparticle solution diluted 50-fold onto a formvar/carbon-supported Cu grid (Ted Pella). High-resolution TEM image and electron diffraction pattern were acquired using an FEI Tecnai-G2-20 TEM. Morphological and topographical information were obtained by a Hitachi S4800 scanning electron microscope (SEM) operating

at 5 kV and a Digital Instruments Dimension-3100 atomic force microscope (AFM) operating in tapping mode. Magnetic properties were studied at room temperature using a MicroSense EZ high-sensitivity vibration sample magnetometer (VSM) with maximum field of 3 T.

Results and discussion

Synthesis of monodisperse nanoparticles

Cobalt ferrite nanoparticles were selected as the magnetic nanomaterials due to their uniaxial effective magnetic anisotropy (Wen et al. 2017). Nanoparticle synthesis follows the nucleation and growth process in colloidal crystal formation (Jiang et al. 2017a). A multi-step heating method was employed to improve the nanoparticle morphology. As revealed by the TEM image in Fig. 2a, the synthesized monodisperse nanoparticles (size of 9.8 nm, size distribution of 7%) were organized into locally ordered domains with distinct packing patterns, similar to the frustrated grains in stressed polycrystal (Palombo et al. 2013). The oriented arrangement of the nanoparticles can be related to the shape-mediated nature of the spontaneous self-assembly (Lee et al. 2018; Song et al. 2006). The lattice plane distance measured from the high-resolution TEM in Fig. 2b and the lattice spacing calculated from the electron diffraction pattern in Fig. 2c match with the standard powder diffraction data of spinel structured $CoFe_2O_4$ (JCPDS 22-1086). Hysteresis loop of the nanoparticles prepared in pressed pellet was shown in Fig. 2d. The small coercivity (H_c = 5.2 Oe) is presumably attributed to that the nanoparticle size lies in the superparamagnetic regime. The reduced saturation magnetization of the nanoparticles (M_s = 46 emu g^{-1}) compared with the bulk counterpart (M_s = 94 emu g^{-1}) can be related to antiphase boundary defect, surface oxidation, and spin canting effect (McKenna et al. 2014; Jiang et al. 2017b). Replacing the benzyl ether with octadecene in the synthesis protocol led to polydisperse nanoparticles with similar shape (8–12 nm, polyhedral) but different magnetic properties (M_s = 74 emu g^{-1}). This finding implies that the organic solvent affects the morphology and associated magnetocrystalline anisotropy of the nanocrystals during their formation.

Fabrication of patterned arrays from nanoparticle film

As illustrated in Fig. 1 a and b, the chemically synthesized nanoparticles were first prepared into a solid film through improved interfacial assembly method under magnetic field (Dong et al. 2010). Initially, nanoparticle solvent was dropped onto the water surface, producing a liquid film. Evaporation of the volatile organic solvent occurred at the three-phase drying front (Kinge et al. 2008). Consequently, the colloidal nanoparticles capped by surfactant were continuously assembled into a solid film under van der Waals and Coulombic interactions (Dong et al. 2010; Wen and Majetich 2011). The rate and direction of solvent evaporation were experimentally controlled, so that an equilibrium state of nanoparticle assembly was reached, as evidenced by the constant movement speed of the drying front on water surface. Mixture of toluene and hexane was used as the carrier solvent in order to tune the solvent volatility and interfacial energy (Wen and Majetich 2011). Note that the nanoparticle-assembled films spontaneously formed in the absence of guiding field usually possess ruptures and cracks. Conventional Langmuir-Blodgett deposition technique applies isothermal compression to eliminate these defects, but undesired stacking or folding structures will be produced (Tao et al. 2008). In our setup, the assembly process was modulated by both the liquid flux and the applied field during solvent evaporation, which helped to improve continuity of the nanoparticle-assembled film and reduce structural defects. Under applied magnetic field, the magnetization directions of the nanoparticles tend to relax to the field direction (Wen et al. 2017). In our case, the magnetization relaxation mechanism is presumably a combination of Néel relaxation and Brownian relaxation, considering the size of nanoparticles, the magnitude of guiding field, and the duration of nanoparticle assembly (Zhang et al. 1996; Wen et al. 2010).

The nanoparticle-assembled film was readily transferred to Si substrate, and a femtosecond laser fabrication platform was utilized to create patterns, as illustrated in Fig. 1 c and d. Preliminary test of line patterning was performed to investigate the feasibility of removing materials from the nanoparticle-assembled film (Fig. 3a). As shown in Fig. 3b, parallel line stripes with various widths (3–6 μm) were produced under different laser pulse energy (100–180 nJ/pulse). It can be inferred that high-energy laser led to thermal diffusion and thermal ablation of non-irradiated nanoparticles (Liao et al.

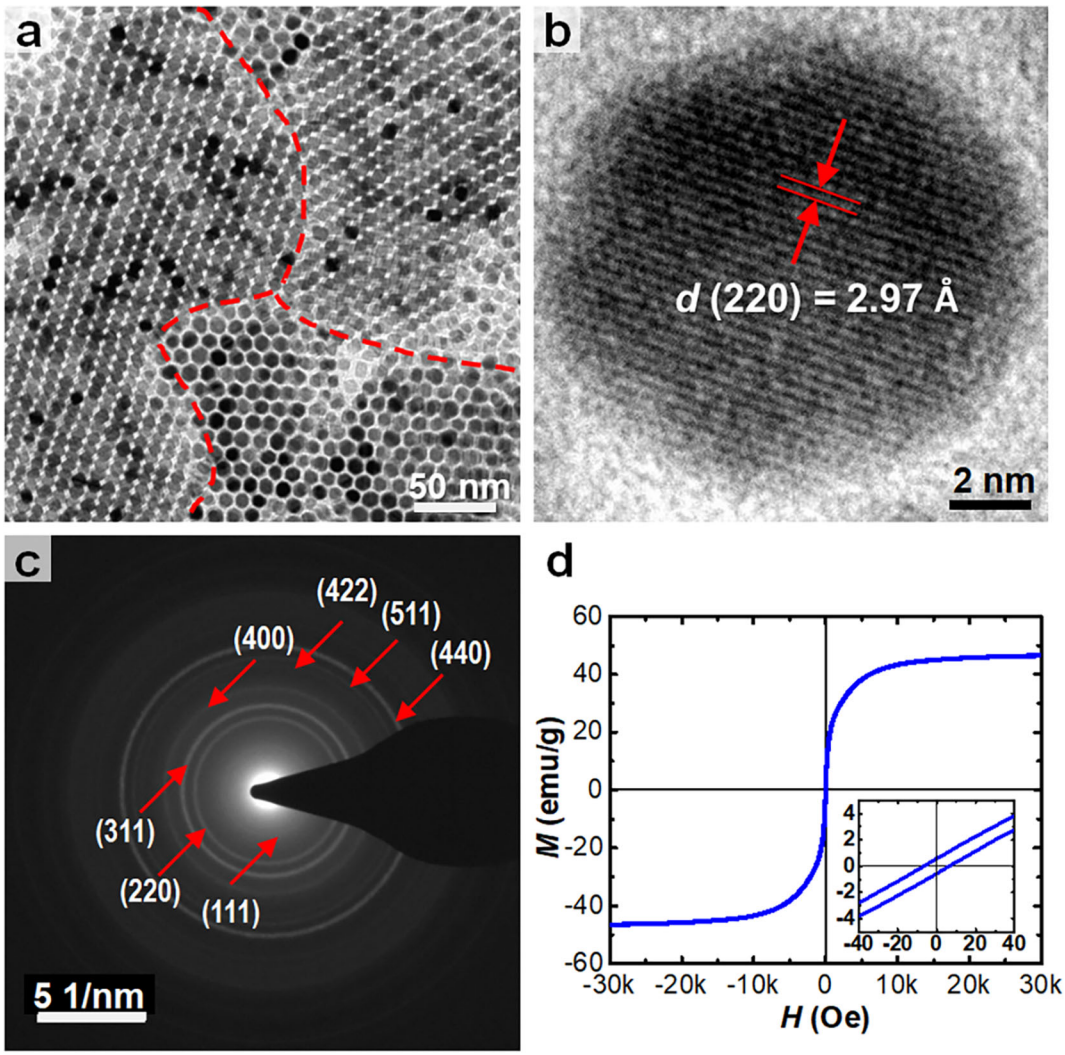

Fig. 2 TEM image (**a**), high-resolution TEM image (**b**), electron diffraction pattern (**c**), and hysteresis loop (**d**) of the as-synthesized $CoFe_2O_4$ nanoparticles

2018; Luft et al. 1996) around the focused laser spot (diameter of 3.1 μm), and the width of the patterned lines (with a minimum size of 3 μm) highly depends on the laser pulse energy. The laser irradiated region with reddish-purple color corresponds to the bare substrate (thermally oxidized silicon). The non-irradiated region with yellowish-green color is the nanoparticle-assembled film, which was closely attached on substrate surface and possessed certain mechanical robustness. Further increasing the laser pulse energy to 250 nJ/pulse resulted in severe damage of the Si substrate, indicating that 250 nJ/pulse is above the ablation threshold of the Si substrate. During microstructure patterning, the laser pulse energy was carefully adjusted within a narrow range of 110–160 nJ/pulse, so that the laser intensity is enough for ablating assembled nanoparticles but not damaging Si surface (the results were examined by SEM in the following part). As shown in Fig. 3c, uniform square array with size of 4 μm and pitch of 8 μm was obtained by scanning the laser beam in two orthogonal directions, and structural consistency was achieved. It was found that residue dusts with size close to 1 μm formed by aggregated nanoparticles (results not shown here) were generated during laser irradiation, and our experimental results show that exhaust ventilation and post-fabrication ultrasonication help to remove most of the micro-sized dusts from the sample surface. Furthermore, square arrays with different size and pitch

were fabricated by either increasing the laser pulse energy (Fig. 3d) or elongating the pitch distance (Fig. 3d inset). As presented in Fig. 3e, bar array in uniform morphology (pitch 12 and 6 μm along x and y directions, respectively) was produced. The length of 9 μm and the width of 3 μm correspond to aspect ratio of 3:1. Moreover, by altering the laser pulse energy (Fig. 3f) or the pitch length (Fig. 3f inset), bar arrays with distinct aspect ratio and size were obtained. As shown in Fig. 3g, antidot array with dot size of 3 μm (pitch 5 μm, roundness 1.01) was fabricated by discretely patterning individual antidots. By changing fabrication parameters, antidot array with different size (Fig. 3g inset) was prepared. In all the patterned arrays, the row number was controlled to be the same as the column number, and the minimum feature size achieved is 1.8 μm. We further perform one-step fabrication of two-dimensional code and data matrix. As presented in Fig. 3h, well-defined QR codes with various dot size (3–4 μm) and pattern size (62–85 μm) were created, and they were successfully read by a smartphone. These user-defined code patterns composed of functional nanoparticles can find applications in information carrier and advanced anticounterfeiting (Wu et al. 2015; You et al. 2015).

By repeating the laser patterning operation on a batch of nanoparticle-assembled films with the same thickness, the variation of array size among different samples is approximately 10%. The average fabrication time for creating typical square array (total number of $\sim 3.9 \times 10^5$, pitch distance of 8 μm) on a 25 mm^2 substrate is 11 min. Note that the laser pulse frequency limits the maximum scanning speed of laser beam, since too fast scanning speed will generate discontinuous patterns due to the pulsing nature of the laser source. The thickness of patterned array was readily increased by adjusting the nanoparticle solution concentration (from 25 to 50 mg mL^{-1}) when preparing the nanoparticle-assembled film. The resulting structures have different colors ranging from yellowish green (Fig. 3c) to dark yellow (Fig. 3c inset), which correspond to film thickness of around 50 nm and 90 nm, respectively.

The square array sample in Fig. 3c inset (pitch of 8 μm, size of 4 μm) was further characterized by SEM, as shown in Fig. 4a. The square array depicted by contrast difference has nearly the same shape. Close-up SEM in Fig. 4b reveals the morphology of a single microstructure in the square array. Besides, a transitional region was observed around the microstructure and the nanoparticles were partially removed, which may be attributed to that the energy density of the laser spot has gradient distribution. The non-irradiated region and irradiated region were further examined under SEM, as shown in Fig. 4 c and d, respectively. In the non-irradiated region, the assembled nanoparticles have fine texture, illustrating that the nanoparticle-assembled film composed of densely packed particles is free from defect and vacancy. In the irradiated region, one layer of sparsely distributed nanoparticles was observed, and the top surface of Si substrate was not damaged. These remaining nanoparticles were individually resolved by SEM and nanoparticle sintering or coalescence were not observed, and similar research works on interfacial assembly suggest that the surfactant-capped nanoparticles were closely attached on Si surface by electrostatic interaction (Oberdick and Majetich 2013). Surface treatment of the Si substrate before nanoparticle assembly and liquid immersion of the sample during laser irradiation may help to reduce the electrostatic attachment of the nanoparticles on Si surface and clean the ablated nanoparticles in the irradiated region (Shen et al. 2008). The AFM image in Fig. 4e reveals that the square array has well-defined edges and the measured thickness is 89 nm, corresponding to around 9 layers of nanoparticles. It is noticed that the uniformity of the patterned squares is not high and their edges are not sharp enough, and this is probably due to the discontinuous pulsing feature the femtosecond laser and the thermal diffusion of the nanomaterial. Modifying the laser fabrication method by using 3D laser ablation apparatus, multi-step ablation process, or liquid immersion technique (Liao et al. 2018; Shen et al. 2008) could improve the patterning precision and produce uniform geometric features. The cross-section plot in Fig. 4f extracted from the AFM image illustrates the repeating lateral profile of the square array. These characterization results indicate that the laser patterning process presumably utilizes laser ablation to selectively remove the surfactant-capped metal oxide nanoparticles by evaporation (Gruzdev et al. 2011; Gamaly et al. 2002).

Collective properties of the patterned arrays of assembled nanoparticles

The assembled nanoparticles in the patterned array have uniform spacing and determined geometry, and their arrangement, morphology, and composition can be manipulated in a controlled manner. From the viewpoint of magnetism, the microstructure array composed of

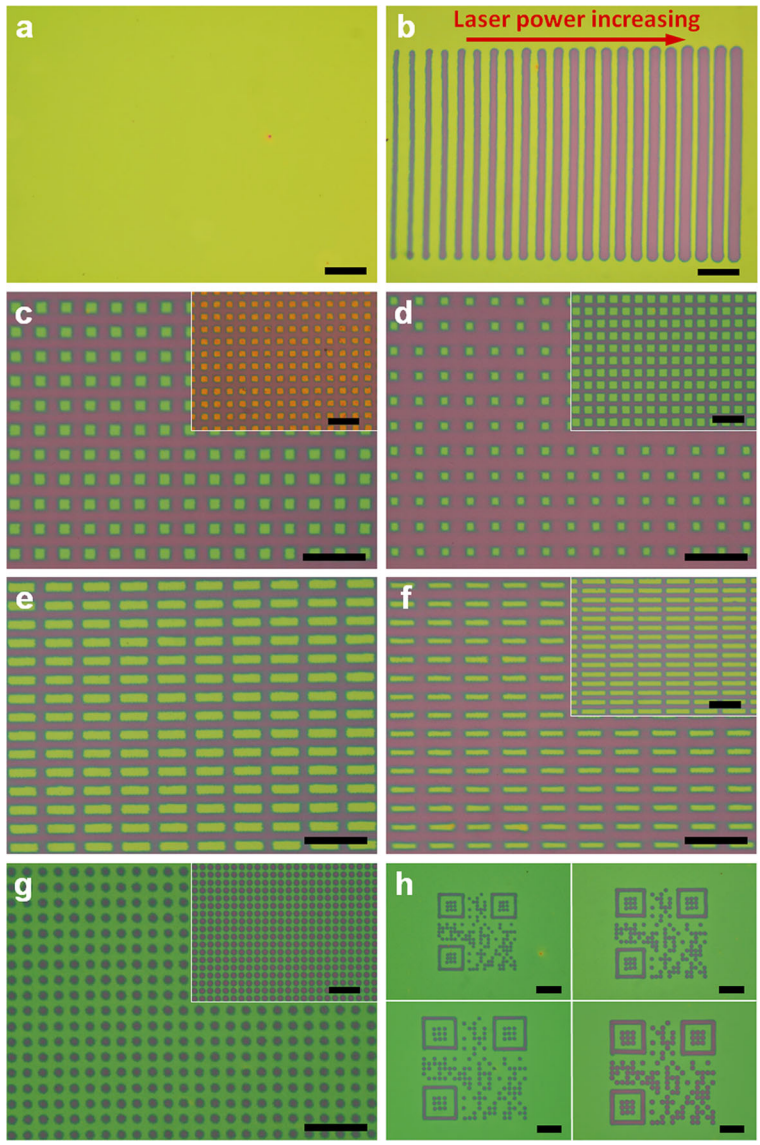

Fig. 3 Optical microscopy images of nanoparticle-assembled film before laser patterning (**a**), line stripes fabricated under different laser pulse energy (**b**), patterned square arrays with different geometry (**c**, **d**), patterned bar arrays with different geometry (**e**, **f**), patterned antidot arrays with different geometry (**g**), and patterned QR codes with different geometry carrying text information of "Nagoya University" (**h**). All scale bars are 20 μm

magnetic nanomaterials is an intriguing particle system, in which the collective magnetic properties of individual microstructures can be investigated by measuring the total response of the microstructure array (Wen et al. 2015). Under applied magnetic field, the magnetic interactions between separated microstructures are quite weak due to their large distance up to several microns, whereas sufficiently strong dipolar interactions exist among the closely packed nanoparticles in each microstructure (Pauly et al. 2012). Herein, two samples of square arrays (size of 4 μm, pitch of 8 μm) with same pattern but different thickness were studied. Field-dependent magnetization curves (hysteresis loops) of the two samples before and after laser patterning were acquired in order to investigate how the patterning process and the sample thickness affect the collective magnetic properties.

The first sample (Fig. 3c) was prepared from a nanoparticle-assembled film with 51 nm thickness. As presented in Fig. 5a, the pristine film without laser patterning shows in-plane magnetic anisotropy, which is reflected by the larger coercivity and steeper slope of the in-plane magnetization curve compared with the out-of-plane one. Besides, at maximum field of 3 T, the measured value of in-plane saturation magnetization ($M_s = 3.0 \times 10^{-4}$ emu) is larger than the out-of-plane

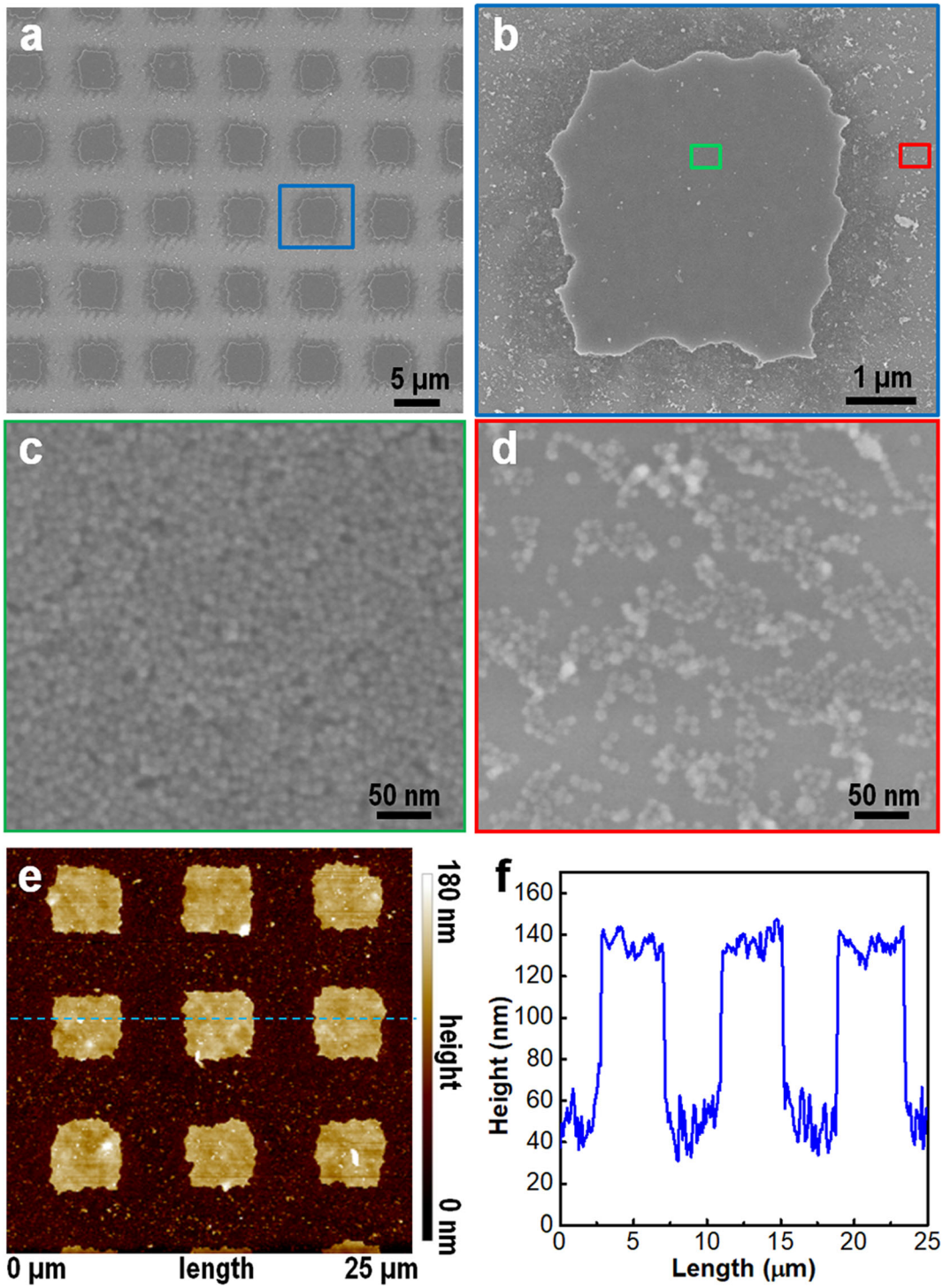

Fig. 4 SEM image (**a**), close-up SEM image (**b**), magnified SEM image in the non-irradiated region (**c**), magnified SEM image in the irradiated region (**d**), AFM image (**e**), and cross-section profile (**f**) of the patterned square array of assembled nanoparticles. Array pitch and array size are 8 μm and 4 μm, respectively

value ($M_s = 2.6 \times 10^{-4}$ emu). These observations indicate that 2D shape anisotropy of the nanoparticle-assembled film can be considered as the dominating factor leading to the preferential orientation of nanoparticles' magnetic moments along the in-plane direction (Toulemon et al. 2016a), and hence the easy axis of the nanoparticle-assembled film is located along in-plane direction. Moreover, considering the intrinsic dipolar interactions, magnetization reversal in nanoparticle-assembled film presumably occurs through in-plane rotation (Pauly et al. 2012). Such magnetization behavior is quite different from the case of disordered powder sample of nanoparticles (Fig. 2d), in which the magnetization reversal occurs in any direction (Pauly et al. 2012; Pichon et al. 2014). After patterning this nanoparticle-assembled film into square array (Fig. 5b), the in-plane coercivity remained almost unchanged, whereas the out-of-plane coercivity increased from 8.2 to 12.5 Oe. Note that the coercive field is associated with the energy barrier required for aligning nanoparticles' magnetic moments upon magnetic field reversal (Majetich and Sachan 2006). On the other hand, the squareness (M_r/M_s) and the slope of the out-of-plane magnetization curve were also increased. In literature, the squareness of nanoparticle system was reported to be strongly affected by the dimensionality of assembled nanoparticles and the interparticle distance (Toulemon et al. 2016a; Held et al. 2001). In our case, such enhancement of both coercivity and squareness in the out-of-plane direction is related to the laser patterning process. Essentially, the continuous film with millimeter size (5 by 5 mm) was patterned into magnetically decoupled array with micron size (4 by 4 μm). Such shape anisotropy change resulted in the enhancement of magnetic anisotropy along out-of-plane direction. The significant decrease of the saturation magnetization (M_s) in both in-plane and out-of-plane directions was due to the removal of magnetic materials.

The second sample (Fig. 3c inset) was prepared from a nanoparticle-assembled film with 89 nm thickness. The magnetization curve in Fig. 5c also reveals a preferential in-plane magnetization in the pristine film. After patterning into square array (Fig. 5d), the in-plane coercivity of this sample changed slightly while the out-of-plane coercivity exhibited a notable rise from 8.7 to 14.3 Oe. The squareness of the out-of-plane magnetization curve tended to increase as well. Compared with the previous sample with small thickness, this sample with large thickness exhibits more pronounced improvement of magnetic anisotropy along out-of-plane direction. Thus, it can be inferred that by increasing the thickness of nanoparticle-assembled film or alternatively by reducing the size of patterned array, the shape anisotropy will be modified to promote the out-of-plane magnetic anisotropy. These results can provide guidelines for tuning the collective magnetic properties and magnetization behaviors of nanoparticle-assembled structures.

As for our patterned array of assembled nanoparticles, the overall magnetic anisotropy was determined by the competition between the shape anisotropy induced by laser patterning and the magnetocrystalline anisotropy induced by guiding field. The increase of out-of-plane magnetic anisotropy after laser patterning is presumably related to the shape anisotropy change. The magnetic anisotropy can also be promoted along out-of-plane direction by increasing the out-of-plane guiding field applied during nanoparticle assembly process, which enhances the out-of-plane magnetocrystalline anisotropy (Duong et al. 2014). In non-interacting ensembles of single-domain magnetic nanoparticles, each nanoparticle can be considered as a magnetic dipole with single magnetic moment (Majetich and Sachan 2006; Bedanta and Kleemann 2008). At finite temperature, magnetization of a nanoparticle reverses its direction along the magnetic easy axis by means of thermal agitation within a characteristic relaxation time τ, described by the Néel-Arrhenius equation:

$$\tau = \tau_0 \exp(E_a/k_B T) \quad (1)$$

where T is absolute temperature, k_B is Boltzmann constant, τ_0 is the material-specific attempt time, and E_a is the magnetic anisotropy energy (Pauly et al. 2012; Dormann et al. 1997; Wernsdorfer 2001). In compact ensembles of single-domain nanoparticles with sufficiently strong dipole interactions, both the magnetic anisotropy energy (E_a) and dipole energy (E_d) are important in determining the collective magnetic properties and the magnetization reversal behaviors (Held et al. 2001; Duong et al. 2014). Further works on temperature-dependent measurement of zero-field-cooled and field-cooled (ZFC/FC) magnetization curves need to be done to study the energy-related properties of the assembled nanoparticles (Majetich and Sachan 2006; Fleutot et al. 2013).

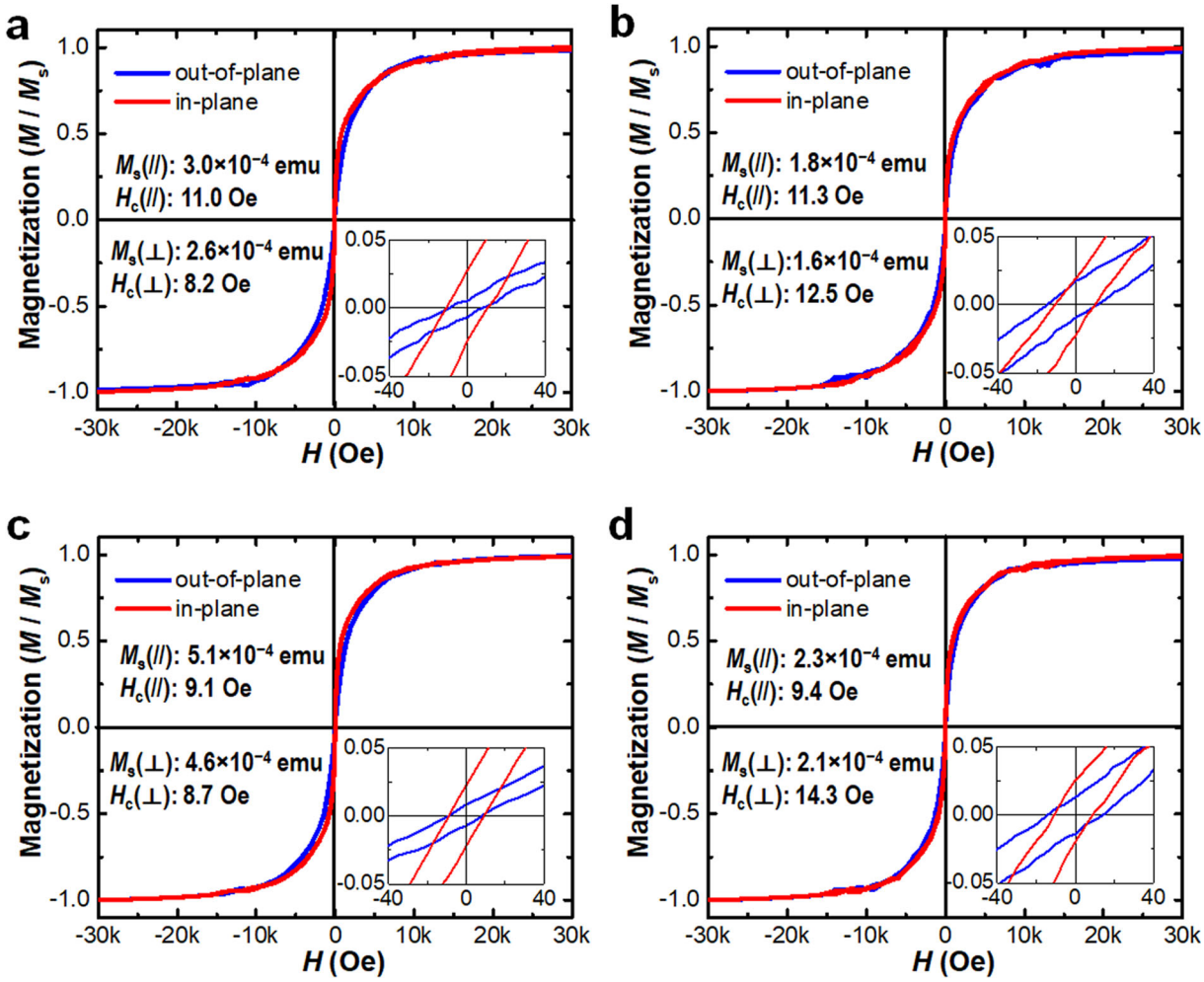

Fig. 5 Hysteresis loops of nanoparticle-assembled film with 51 nm thickness before laser patterning (**a**) and after patterning into square array (**b**). Hysteresis loops of nanoparticle-assembled film with 89 nm thickness before laser patterning (**c**) and after patterning into square array (**d**). Sample area: 25 mm^2; array pitch: 8 μm; array size: 4 μm. M_s and H_c represent saturation magnetization and coercivity, respectively

Conclusion

In conclusion, we have developed a novel fabrication protocol for creating patterned arrays of assembled nanoparticles. Uniform microstructure arrays and customized QR codes with various geometry were produced by patterning nanoparticle-assembled film on Si substrate. The field-guided interfacial assembly improved the structural continuity of nanoparticle-assembled film, and the femtosecond laser patterning enables the selective material removal at high resolution. The size, shape, and spacing of the patterned array were regulated in a controlled manner. Magnetization measurements reveal that the out-of-plane magnetic anisotropy of the magnetically decoupled arrays was enhanced after laser patterning due to their shape anisotropy change. The presented fabrication protocol is maskless and template-free, and it can be further applied to other inorganic nanoparticles for studying the collective properties of nanoparticle-assembled structures and developing nanomaterial-based devices (Zuo et al. 2019).

Author contributions The manuscript was written through contributions of all authors. All authors have given approval to the final version of the manuscript.

Funding information This work was supported by "Nanotechnology Platform Program" sponsored by the Ministry of Education, Culture, Sports, Science and Technology (MEXT), Japan. PWP

acknowledges support from ITF Tier 3 funding (ITS/203/14, ITS/104/13, ITS/214/14), RGC-GRF grant (HKU 17210014, HKU 17204617), and UGC Hong Kong (contract no. AoE/P-04/08).

Compliance with ethical standards

Conflict of interest The authors declare that they have no conflict of interest.

References

Bedanta S, Kleemann W (2008) Supermagnetism. J Phys D Appl Phys 42:013001

Boles MA, Engel M, Talapin DV (2016) Self-assembly of colloidal nanocrystals: from intricate structures to functional materials. Chem Rev 116:11220–11289

Boyd RW (2003) Nonlinear optics, 3rd edn. Rochester, New York

Catone D, Ciavardini A, Di Mario L et al (2018) Plasmon controlled shaping of metal nanoparticle aggregates by femtosecond laser-induced melting. J Phys Chem Lett 9:5002–5008

Cheang UK, Kim MJ (2015) Self-assembly of robotic micro-and nanoswimmers using magnetic nanoparticles. J Nanopart Res 17:145

Chiang WY, Chen JJK, Usman A et al (2019) Formation mechanism and fluorescence characterization of a transient assembly of nanoparticles generated by femtosecond laser trapping. J Phys Chem C. https://doi.org/10.1021/acs.jpcc.9b04471

Dong A, Chen J, Vora PM et al (2010) Binary nanocrystal superlattice membranes self-assembled at the liquid–air interface. Nature 466:474

Dormann J-L, Fiorani D, Tronc E (1997) Magnetic relaxation in fine-particle systems. Adv Chem Phys 1997:283–494. https://doi.org/10.1002/9780470141571.ch4

Duong B, Khurshid H, Gangopadhyay P, Devkota J, Stojak K, Srikanth H, Tetard L, Norwood RA, Peyghambarian N, Phan MH, Thomas J (2014) Enhanced magnetism in highly ordered magnetite nanoparticle-filled nanohole arrays. Small 10:2840–2848

Flauraud V, Mastrangeli M, Bernasconi GD et al (2017) Nanoscale topographical control of capillary assembly of nanoparticles. Nat Nanotechnol 12:73

Fleutot S, Nealon GL, Pauly M, Pichon BP, Leuvrey C, Drillon M, Gallani JL, Guillon D, Donnio B, Begin-Colin S (2013) Spacing-dependent dipolar interactions in dendronized magnetic iron oxide nanoparticle 2D arrays and powders. Nanoscale 5:1507–1516

Gamaly EG, Rode AV, Luther-Davies B et al (2002) Ablation of solids by femtosecond lasers: ablation mechanism and ablation thresholds for metals and dielectrics. Phys Plasmas 9:949–957

Gassensmith JJ, Erne PM, Paxton WF, Frasconi M, Donakowski MD, Stoddart JF (2013) Patterned assembly of quantum dots onto surfaces modified with click microcontact printing. Adv Mater 25:223–226

Gruzdev V, Komolov V, Li H et al (2011) Photo-ionization and modification of nanoparticles on transparent substrates by ultrashort laser pulses. Proc SPIE 7996:79960J

Held G, Grinstein G, Doyle H et al (2001) Competing interactions in dispersions of superparamagnetic nanoparticles. Phys Rev B 64:012408

Ionin AA, Kudryashov SI, Makarov SV et al (2014) Structural and electrical characteristics of a hyperdoped silicon surface layer with deep donor sulfur states. JETP Lett 100:55–58

Jiang C, Chan PH, Leung CW et al (2017a) $CoFe_2O_4$ nanoparticle-integrated spin-valve thin films prepared by interfacial self-assembly. J Phys Chem C 121:22508–22516

Jiang C, Ng SM, Leung CW et al (2017b) Magnetically assembled iron oxide nanoparticle coatings and their integration with pseudo-spin-valve thin films. J Mater Chem C 5:252–263

Jie Y, Niskala JR, Johnston-Peck AC et al (2012) Laterally patterned magnetic nanoparticles. J Mater Chem 22:1962–1968

Kang B, Han S, Kim J et al (2011) One-step fabrication of copper electrode by laser-induced direct local reduction and agglomeration of copper oxide nanoparticle. J Phys Chem C 115:23664–23670

Kinge S, Crego-Calama M, Reinhoudt DN (2008) Self-assembling nanoparticles at surfaces and interfaces. Chem Phys Chem 9:20–42

Kudryashov SI, Nguyen LV, Kirilenko DA et al (2018) Large-scale laser fabrication of antifouling silicon-surface nanosheet arrays via nanoplasmonic ablative self-organization in liquid CS_2 tracked by a sulfur dopant. ACS Appl Nano Mater 1:2461–2468

Lan S, Wu X, Zhang G et al (2019) Improvement of device performance of organic photovoltaics via laser irradiation. J Phys Chem C 123:22058–22065

Lee D, Paeng D, Park HK, Grigoropoulos CP (2014) Vacuum-free, maskless patterning of Ni electrodes by laser reductive sintering of NiO nanoparticle ink and its application to transparent conductors. ACS Nano 8:9807–9814

Lee YH, Lay CL, Shi W et al (2018) Creating two self-assembly micro-environments to achieve supercrystals with dual structures using polyhedral nanoparticles. Nat Commun 9:2769

Liao C, Anderson W, Antaw F et al (2018) Maskless 3D ablation of precise microhole structures in plastics using femtosecond laser pulses. ACS Appl Mater Interfaces 10:4315–4323

Lin CH, Zeng Q, Lafalce E et al (2018) Large-area lasing and multicolor perovskite quantum dot patterns. Adv Opt Mater 6:1800474

Luft A, Franz U, Emsermann L et al (1996) A study of thermal and mechanical effects on materials induced by pulsed laser drilling. Appl Phys A Mater Sci Process 63:93–101

Mahajan A, Frisbie CD, Francis LF (2013) Optimization of aerosol jet printing for high-resolution, high-aspect ratio silver lines. ACS Appl Mater Interfaces 5:4856–4864

Majetich S, Sachan M (2006) Magnetostatic interactions in magnetic nanoparticle assemblies: energy, time and length scales. J Phys D Appl Phys 39:R407

McKenna KP, Hofer F, Gilks D et al (2014) Atomic-scale structure and properties of highly stable antiphase boundary defects in Fe3O4. Nat Commun 5:5740

Oberdick SD, Majetich SA (2013) Electrophoretic deposition of iron oxide nanoparticles on templates. J Phys Chem C 117:18709–18718

O'Brien MN, Lin H-X, Girard M et al (2016) Programming colloidal crystal habit with anisotropic nanoparticle building blocks and DNA bonds. J Am Chem Soc 138:14562–14565

Okamoto T, Nakamura T, Sakota K, Yatsuhashi T (2019) Synthesis of single-nanometer-sized gold nanoparticles in liquid–liquid dispersion system by femtosecond laser irradiation. Langmuir 35:12123–12129

Paik T, Yun H, Fleury B, Hong SH, Jo PS, Wu Y, Oh SJ, Cargnello M, Yang H, Murray CB, Kagan CR (2017) Hierarchical materials design by pattern transfer printing of self-assembled binary nanocrystal superlattices. Nano Lett 17: 1387–1394

Palombo M, Gabrielli A, Servedio V et al (2013) Structural disorder and anomalous diffusion in random packing of spheres. Sci Rep 3:2631

Pauly M, Pichon BP, Panissod P et al (2012) Size dependent dipolar interactions in iron oxide nanoparticle monolayer and multilayer Langmuir–Blodgett films. J Mater Chem 22: 6343–6350

Pichon BP, Leuvey C, Ihawakrim D et al (2014) Magnetic properties of mono-and multilayer assemblies of iron oxide nanoparticles promoted by SAMs. J Phys Chem C 118:3828–3837

Polavarapu L, Liz-Marzán LM (2013) Towards low-cost flexible substrates for nanoplasmonic sensing. Phys Chem Chem Phys 15:5288–5300

Shen M, Carey JE, Crouch CH, Kandyla M, Stone HA, Mazur E (2008) High-density regular arrays of nanometer-scale rods formed on silicon surfaces via femtosecond laser irradiation in water. Nano Lett 8:2087–2091

Son Y, Yeo J, Moon H, Lim TW, Hong S, Nam KH, Yoo S, Grigoropoulos CP, Yang DY, Ko SH (2011) Nanoscale electronics: digital fabrication by direct femtosecond laser processing of metal nanoparticles. Adv Mater 23:3176–3181

Song Q, Ding Y, Wang ZL, Zhang ZJ (2006) Formation of orientation-ordered superlattices of magnetite magnetic nanocrystals from shape-segregated self-assemblies. J Phys Chem B 110:25547–25550

Stratakis E, Barberoglou M, Fotakis C, Viau G, Garcia C, Shafeev GA (2009) Generation of Al nanoparticles via ablation of bulk Al in liquids with short laser pulses. Opt Express 17: 12650–12659

Tao AR, Huang J, Yang P (2008) Langmuir−Blodgettry of nanocrystals and nanowires. Acc Chem Res 41:1662–1673

Tian Y, Wang T, Liu W et al (2015) Prescribed nanoparticle cluster architectures and low-dimensional arrays built using octahedral DNA origami frames. Nat Nanotechnol 10:637

Toulemon D, Liu Y, Cattoën X, Leuvrey C, Bégin-Colin S, Pichon BP (2016a) Enhanced collective magnetic properties in 2D monolayers of iron oxide nanoparticles favored by local order and local 1D shape anisotropy. Langmuir 32:1621–1628

Toulemon D, Rastei MV, Schmool D (2016b) Enhanced collective magnetic properties induced by the controlled assembly of iron oxide nanoparticles in chains. Adv Funct Mater 26: 2454–2462

Wang X, Pu J, An B et al (2018) Programming cells for dynamic assembly of inorganic nano-objects with spatiotemporal control. Adv Mater 30:1705968

Wang J-P (2008) FePt magnetic nanoparticles and their assembly for future magnetic media. Proc IEEE 96:1847–1863

Wen T, Li Y, Zhang D, Zhan Q, Wen Q, Liao Y, Xie Y, Zhang H, Liu C, Jin L, Liu Y, Zhou T, Zhong Z (2017) Manipulate the magnetic anisotropy of nanoparticle assemblies in arrays. J Colloid Interface Sci 497:14–22

Wen T, Liang W, Krishnan KM (2010) Coupling of blocking and melting in cobalt ferrofluids. J Appl Phys 107:09B501. https://doi.org/10.1063/1.3350901

Wen T, Majetich SA (2011) Ultra-large-area self-assembled monolayers of nanoparticles. ACS Nano 5:8868–8876

Wen T, Zhang D, Wen Q, Zhang H, Liao Y, Li Q, Yang Q, Bai F, Zhong Z (2015) Magnetic nanoparticle assembly arrays prepared by hierarchical self-assembly on a patterned surface. Nanoscale 7:4906–4911

Wernsdorfer W (2001) Classical and quantum magnetization reversal studied in nanometer-sized particles and clusters. Adv Chem Phys 118:99–190

Wu L, Dong Z, Kuang M et al (2015) Printing patterned fine 3D structures by manipulating the three phase contact line. Adv Funct Mater 25:2237–2242

You M, Zhong J, Hong Y, Duan Z, Lin M, Xu F (2015) Inkjet printing of upconversion nanoparticles for anti-counterfeit applications. Nanoscale 7:4423–4431

Zhang J, Boyd C, Luo W (1996) Two mechanisms and a scaling relation for dynamics in ferrofluids. Phys Rev Lett 77:390

Zhang Y, Zhang F, Yan Z et al (2017) Printing, folding and assembly methods for forming 3D mesostructures in advanced materials. Nat Rev Mater 2:17019

Zuo P, Jiang L, Li X et al (2019) Maskless micro/nanopatterning and bipolar electrical-rectification of MoS_2 flakes through femtosecond laser direct writing. ACS Appl Mater Interfaces 11:39334–39341